13

Phase Correlation of Electrons and Langmuir Waves

C.A. Kletzing[1] and L. Muschietti[2]

[1] Department of Physics and Astronomy, University of Iowa
craig-kletzing@uiowa.edu
[2] Space Sciences Lab., University of California
laurent@ssl.berkeley.edu

Abstract. Multiple spacecraft observations have confirmed the ubiquitous nature of Langmuir waves in the presence of auroral electrons. The electrons show variations consistent with bunching at or near the plasma frequency. Linear analysis of the interaction of a finite Gaussian packet of Langmuir waves shows that there are two components to the perturbation to the electron distribution function, one in-phase (or 180° out-of-phase) with respect to the wave electric field called the resistive component and one which is 90° (or 270°) out-of-phase with respect to the electric field. For small wave packets, the resistive perturbation dominates. For longer wave packets, a non-linear analysis is appropriate which suggests that the electrons become trapped and the reactive phase dominates. Rocket observations have measured both components. The UI observations differ from those of the UC Berkeley observations in that a purely reactive phase bunching was observed as compared to a predominantly resistive perturbation. The resistive phase results of the UC Berkeley group were interpreted as arising from a short wave packet. The UI observations of the reactive phase can be explained by either a long, coherent train of Langmuir waves or that the narrower velocity response of the UI detectors made it possible to capture only one side of the reactive component of the perturbed distribution function for a short wave packet in the linear regime. Future wave-particle correlator experiments should be able to resolve these questions by providing more examples with better velocity space coverage.

Key words: Electron bunching, Langmuir waves, resistive and reactive bunching phases, phase correlators

13.1 Introduction

The precipitation of auroral electrons provides an example of a beam-plasma interaction which generates Langmuir waves from the free energy in the electrons. The resulting waves play several important roles in the Earth's auroral ionosphere. First, the waves Landau damp on the thermal electron population

C.A. Kletzing and L. Muschietti: *Phase Correlation of Electrons and Langmuir Waves*, Lect. Notes Phys. **687**, 313–337 (2006)
www.springerlink.com

and thereby form a direct conduit for energy exchange between the auroral electron beam and the thermal electrons. Several authors have speculated that Langmuir waves play a significant role in establishing the electron temperature in the auroral ionosphere [3, 15]. In addition to heating electrons, the Langmuir/upper hybrid waves radiate away some of their energy into electromagnetic radiation, which can serve for remote sensing of auroral plasma processes from ground level and from satellites. For example, auroral roar is an EM emission observed near 2–3 and 4–4.5 MHz at ground level [14, 30] and from satellites [1, 12].

Understanding these auroral wave emissions is important not only to fully understand terrestrial aurora and related phenomena, but also because they shed light on analogous emission processes elsewhere in the solar system and beyond. For example, the generation of auroral roar is similar to that of terrestrial continuum radiation, which is generated via mode conversion of upper hybrid waves at the plasmapause, and possibly continuum radiations at other planets as well. Solar type III radiation results from mode conversion of Langmuir waves in the solar wind, and recent observations of structured type III emission [Reiner et al., 23, 24] indicate the significance of frequency structure in the causative Langmuir waves.

High frequency (HF) electric field observations in the topside auroral ionosphere, for which the plasma frequency is typically greater than the electron cyclotron frequency, have revealed plasma waves in the range $f_{pe} \leq f \leq f_{uh}$ ever since the earliest measurements [2, 29]. Simultaneous wave and electron distribution measurements have shown that the waves are excited by Landau resonance but that temporal variation of the distribution function or wave refraction from vertical density gradients can limit wave amplitudes as shown by McFadden et al. [19]. Many examples of waves near f_{pe} were observed using Aureol/ARCAD 3 satellite wave receivers and the free-energy source was identified as the electrons [Beghin et al., 3]. Although rocket-borne receivers have detected HF waves at E-region altitudes attributed to generation by secondary electrons [Kelley and Earle, 13], most observations pertain to altitudes from 300 km and up, where the waves have amplitudes ranging from less than 1 mV/m to as large as 1 V/m [4, 6, 8, 17, 18, 28] These waves are highly bursty in time, sometimes lasting as little as 1 ms but sometimes appearing continuous for ∼1s. Recent high-resolution experiments reveal that they can have complex frequency structure [17, 18, 25]. Other investigators have detected plasma waves through particle-particle correlator techniques. Using a rocket-borne electron detector of large geometric factor, ∼5% modulation at frequencies 4.2–5.6 MHz was found during a 7-second interval when the rocket passed the boundary of two oppositely directed Birkeland sheet currents [27]. Strong modulation (∼30%) was observed at 2.65 MHz of 4–5 keV electrons, corresponding to energies at which a positive slope was observed in the perpendicular and parallel velocity distribution functions [Gough and Urban, 11]. Rocket measurements in which 1.4 MHz fluctuations were detected in the 7.5 keV electrons, just below the electron beam energy, were reported to

occur simultaneously with a positive slope in the electron distribution function [Gough et al., 10].

Linear theory explains the existence and parallel polarization of auroral Langmuir waves [see, e.g., Nicholson, 22]. Theory and simulations have shown that Langmuir waves in the auroral plasma most likely do not develop into strong turbulence but that observed non-linear features in amplitudes and modulations of the waves are consistent with nonlinear interactions between the Langmuir waves and ion acoustic waves [Newman et al., 21]. More recently, the difference between Langmuir wave-electron interactions both at rocket altitudes and at the altitude of the Freja spacecraft have been studied, finding that standard quasi-linear diffusion theory does not hold for large amplitude Langmuir waves at Freja altitudes, but should hold at lower altitudes [Sanbonmatsu et al., 26].

Correlating waves and particles directly probes the physics of their interaction by providing a superior picture of the microphysics compared to statistically associating an unstable feature of the distribution function with the presence of waves. Elementary theory implies that if the electrons and the waves are exchanging energy, the electrons will have an oscillatory component at a velocity equal to the phase velocity of the waves. Identifying the velocity at which the electron distribution function has this oscillatory component determines the wave phase velocity and therefore the wave number. Measuring the phase of this oscillatory component of the electron distribution function relative to the wave electric field yields further information. The phase bunching splits into two pieces: 1) the resistive component, in phase with the electric field indicating wave-electron energy exchange; and 2) the reactive component, 90° out of phase with the electric field indicating trapping [Nicholson, 22].

Detailed treatment of phase relationships by Muschietti et al. [20] for Gaussian Langmuir wave packets, show that the linear perturbation in the distribution function may be considered as the sum of a resistive and reactive components. For both components, the perturbation narrows and increases in magnitude as the wave packet length increases. Electron detectors with broad energy resolution can only detect the resistive component because it has only positive polarity and adds over the entire energy range. Detecting the bipolar nature of the reactive component requires narrow energy response ($\Delta v/v \leq 5-6\%$) detectors.

Only three high frequency (MHz) wave-particle correlation experiments have been reported in the literature [7, 9, 16]. Very similar experiments have been tried on FREJA by Boehm et al. [5] and on FAST by Ergun et al. [7] but were limited in phase resolution. The first two of these experiments used a correlator that worked by binning individual detected particles according to the phase of the strongest wave detected by a broadband (0.2–5 MHz) wave receiver [Ergun et al., 7, 9]. The most recent experiment used a correlator which had higher phase resolution and detected electrons bunched 90° out-of-phase with respect to the electric field, suggesting non-linear evolution and trapping of the electrons.

In what follows, we discuss the theory of linear perturbations to the distribution by a Gaussian wave packet and also present the theory of extended wave packets via a BGK analysis. We then describe in detail two of the three high frequency wave-particle correlator measurements referred to above. We then conclude with a discussion of these results in the context of theory.

13.2 Finite-Size Wave Packet in a Vlasov Plasma

Consider a coherent, Langmuir packet propagating in the x direction with a phase $\psi = kx - \omega t$ where the frequency ω is close to the plasma frequency $\omega_{\rm p}$. The wave packet is assumed to be localized, which we specify by a form factor $\eta(x,t)$ which is piecewise continuous, bounded, and vanishing for $x \to \pm\infty$. Its slow time dependence describes the drift due to the group velocity of the Langmuir wave or the growth (or damping) due to the interaction with the electrons. Explicitly, the wave electric field is written as

$$E(x,t) = E_0 \eta(x,t) e^{i\psi} \ + c.c. \tag{13.1}$$

where c.c. is the complex conjugate.

The electrons are assumed to consist of two populations: a dense background and energetic, streaming particles. In the problem that we treat, the density of the energetic electrons is orders of magnitude smaller than the background density, so that only the latter determines the real part of the dispersion relation. The electrons are described by a homogeneous distribution function $F(v)$ which includes velocities around the phase velocity of the Langmuir wave, $\mathrm{v_p} \equiv \omega/k$. Under the influence of the wave field, the streaming population develops a time-dependent, inhomogeneous component $f(x,v,t)$ which satisfies the Vlasov equation

$$\frac{d}{dt} f \equiv \left(\frac{\partial}{\partial t} + v \frac{\partial}{\partial x} \right) f = \frac{eE}{m} \frac{\partial}{\partial v} (F + f) \tag{13.2}$$

where $-e$ and m are the electron charge and mass, respectively. Our goal is to find explicit expressions for $f(x,v,t)$ and to analyze their phases versus the wave phase ψ in view of correlator applications.

In the linear approximation, one neglects the perturbation $\partial f/\partial v$ on the right-hand side of (13.2) and formally integrates the equation,

$$f_L(x,v,t) = \frac{eE_0}{m} \int_{-\infty}^{t} \eta(x',t') e^{i\psi(x',t')} \frac{\partial}{\partial v'} F(v')\, dt' \ + c.c. \tag{13.3}$$

The integration is carried out along the trajectories $x'(t')$, $v'(t')$ that have x and v for end points at $t' = t$, namely $x'(t) = x$ and $v'(t) = v$. The perturbation at large negative times when $x' \to \pm\infty$ is ignored. From (13.3) one sees that the linear perturbation f_L oscillates in time with the same

frequency as the electric field. One also notices that the perturbed distribution depends upon the structure of the form factor η along the past trajectories of the particles, which leads to a phase shift relative to the present wave phase $\psi(x,t)$.

13.2.1 Linear Perturbation of the Electrons

Taking as characteristics the straight trajectories $v'(t') = v$ and $x'(t') = x + v(t'-t)$, where v is constant and positive, one rewrites (13.3) as

$$f_L(x,v,t) = A_0\, e^{i(kx-\omega t)} \frac{\partial F}{\partial v} \int_{-\infty}^{0} \eta(x+v\tau, \tau+t) e^{i(kv-\omega)\tau} d\tau \; + c.c. \quad (13.4)$$

where $A \equiv eE_0/m$. The integral explicitly relates the distribution f_L to the motion of the particles at earlier times, so that the effect of spatial gradients in the electric field amplitude will be directly seen in the resulting phase relation.

Let us for instance consider the simple profile of a square window with a width L,

$$\eta(x) = \begin{cases} 0 & : \text{ if } x < 0 \\ 1 & : \text{ if } 0 < x < L \\ 0 & : \text{ if } x > L \end{cases} \quad (13.5)$$

From (13.4), one readily obtains

$$f_L(x,v,t) = \frac{iAe^{i\psi}}{\omega - kv} \frac{\partial F}{\partial v} \begin{bmatrix} 1-\beta^x & : \text{ if } 0 < x < L \\ \beta^{(x-L)} - \beta^x & : \text{ if } L < x \end{bmatrix} + c.c. \quad (13.6)$$

where $\beta \equiv \exp i(\omega/v - k)$. In the square bracket to the right, the exponents reflect the presence of the boundaries and modify the phase of the perturbation relative to the wave phase ψ. They also yield a ballistic term $\beta^{(x-L)} - \beta^x$ downstream of the interaction region. An important point is that these boundary terms keep the perturbed distribution function of resonant electrons bounded. The usual expression for a plane wave [(13.6) with the square bracket equal to unity] shows the perturbation to have a singularity at resonance, where the assumed linear solution, therefore, breaks down. Instead, the right-hand side for $0 < x < L$ can be expanded for velocities close to the phase velocity $\mathrm{v_p}$. The resulting expression is finite. One can then differentiate it with respect to v and thus evaluate at $v = \mathrm{v_p}$ the derivative we neglected in the linearization of Vlasov equation (13.2). Using the notation $F' \equiv \partial F/\partial v$, the result can be written as

$$\frac{\partial f_L}{\partial v}|_{\mathrm{v_p}} = F'(\mathrm{v_p}) \frac{2A}{\omega \mathrm{v_p}} \left[(\mathrm{v_p} \frac{\partial ln F'}{\partial v} - 1) kx \cos\psi + (kx)^2 \sin\psi \right] \quad (13.7)$$

The term proportional to $\sin\psi$ (thus out of phase with the electric field) is seen to grow quadratically with the distance into the packet. Therefore, the packet must have a finite extent to assure the validity of the linear perturbation,

which we write $(kL)^2 \ll \omega \mathrm{v_p}/(2A)$. This inequality introduces an important parameter to the problem at hand

$$\mu \equiv \frac{2eE_0k}{m}\left(\frac{kL}{\omega}\right)^2 . \tag{13.8}$$

This quantity measures the effect of the localized electric field on the electrons and can be used as a small expansion parameter. We can think of it as the square of the bounce frequency times the transit duration of a resonant particle.

13.2.2 Case of a Gaussian Packet

A more realistic envelope of wavepacket is provided by a Gaussian. In fact, since the dispersion relation of Langmuir waves is quadratic, a Gaussian packet moving at the group velocity describes well a propagating Langmuir packet. Its dispersion time is given by $t_d \approx (L/\lambda_d)^2\omega_\mathrm{p}^{-1}$ with λ_d the Debye length. This time is very long compared to, for example, the transit duration of resonant electrons, $t_t \approx kL\,\omega_\mathrm{p}^{-1}$. For simplicity, we choose here a static form factor

$$\eta(x) = \exp[-x^2/(2L)^2]\,, \tag{13.9}$$

which is justified since for many applications the group velocity u is much smaller than the velocity of resonant electrons, $u/\mathrm{v_p} = 3\,(k\lambda_d)^2 \ll 1$. After substituting (13.9) into (13.4) and some algebra, one obtains

$$f_L(x,v,t) = A\,\eta(x)e^{i(kx-\omega t)}\frac{\partial F}{\partial v}\frac{L}{v}(-i)Z(\xi)\ + c.c. \tag{13.10}$$

where Z is the usual plasma dispersion function, yet has here a completely different argument:

$$\xi = (\omega - kv)\frac{L}{v} - i\frac{x}{2L}\,. \tag{13.11}$$

The real part of the argument is the Doppler-shifted frequency seen by a traversing electron times its transit duration through the wavepacket. It determines the proximity to resonance during the interaction. The imaginary part of the argument describes the position with respect to the center of the packet.

Let us evaluate now (13.10) at the center of the packet. We can define a resonance function that represents the response of the electron distribution to the wave field:

$$R \equiv \frac{-iL}{v}Z(\xi_r) = \frac{L}{v}\left(\sqrt{\pi}e^{-\xi_r^2} - i\,2e^{-\xi_r^2}\int_0^{\xi_r} e^{y^2}dy\right) \tag{13.12}$$

The real part of R, associated with the Gaussian $e^{-\xi_r^2}$, represents the resistive contribution (in phase with the electric field). The imaginary part, associated

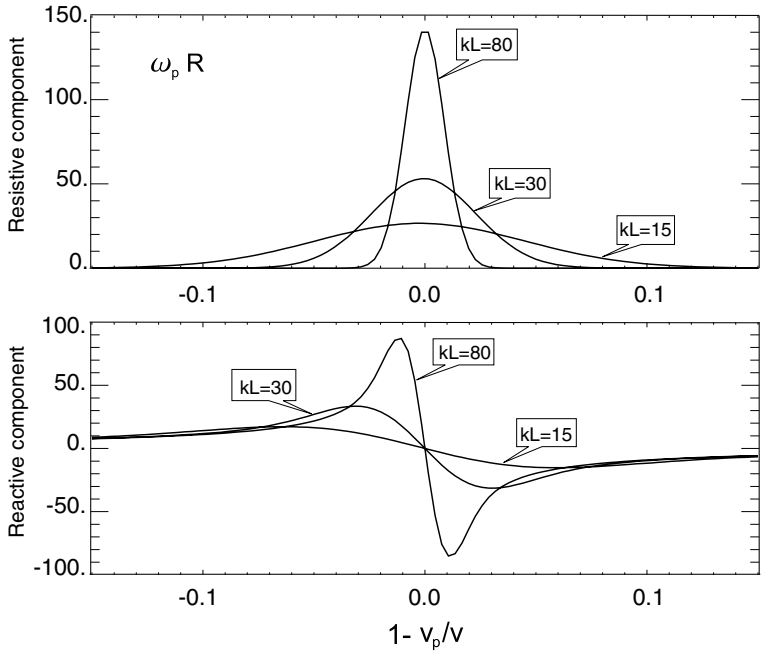

Fig. 13.1. Resonance function defined by (13.12). Real and imaginary parts of R are shown for various packet sizes (Reprinted with permission from American Geophysical Union)

with the Dawson integral, represents the reactive contribution (out of phase with the electric field). When the packet is large so that $\omega L/v \to \infty$, $Re(R)$ tends to the usual delta function of the Plemelj formula, $\pi\delta(kv-\omega)$, and $Im(R)$ tends to the principal part of $1/(kv-\omega)$. Plots of real and imaginary parts of R are displayed in Fig. 13.1 for various sizes of packets. One clearly sees the tendency to a delta function for large kL and, conversely, the broadening of the resonance for a more localized wavepacket.

The perturbed oscillating distribution has components in and out of phase with respect to the electric field. Let us split f_L of (13.10) into resistive and reactive terms, in a way that emulates the procedure performed by the wave correlator on rocket data. One obtains

$$f_L = \frac{\mu}{kL}\frac{\mathrm{v_p^2}}{v}F'(v)\,\eta(x)\,[Z_i\cos(kx-\omega t)+Z_r\sin(kx-\omega t)] \qquad (13.13)$$

where the acceleration factor $A = eE_0/m$ has been rewritten in terms of μ using (13.8). The perturbation is thus either rather resistive or reactive depending upon the relative weight of Z_i and Z_r. Its amplitude is proportional to the wave amplitude, to the packet size, and to the slope of the distribution F. Figure 13.2 displays the perturbation in phase space by means of contours. Solid contours with gray shadings indicate a positive value, i.e. an

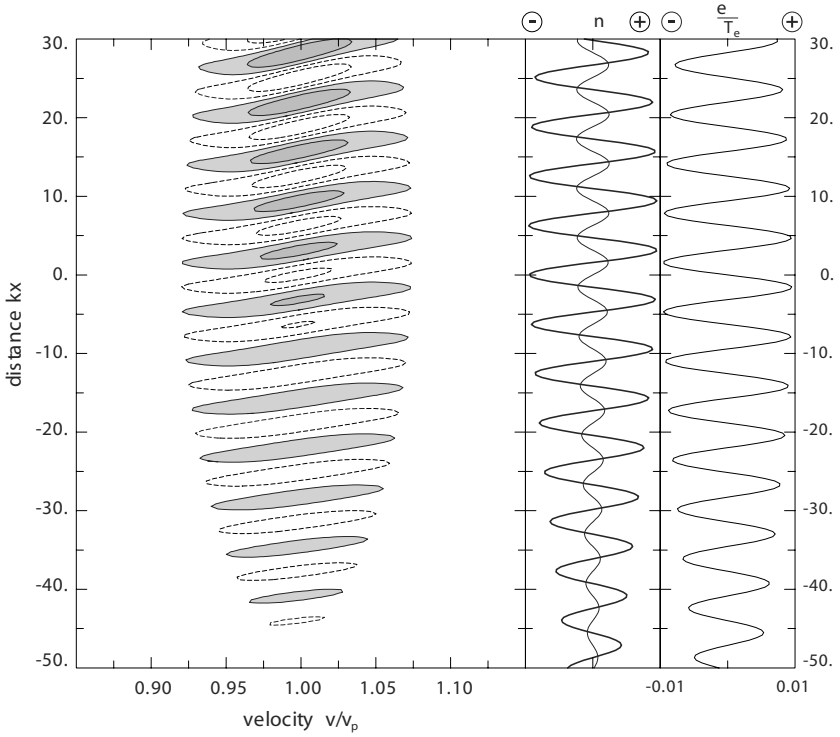

Fig. 13.2. Linear perturbed distribution as described by (13.13) with power-law model $F(v) \sim v^{-4}$. Contours with gray shadings indicate enhancements at levels 0.006 (light) and 0.018 (dark). Dashed contours denote depletions at levels -0.006 and -0.018. The perturbation (normalized to $F(\mathrm{v_p})$) features a chain of bunch-ellipses centered at the phase velocity $\mathrm{v_p}$. Panel marked δn at right displays the resonant density perturbation, split into its resistive (*thick line*) and reactive (*thin line*) components. Rightmost panel shows the potential ϕ of the Langmuir packet with characteristics: $kL = 30$, $\mu = 0.09$

accumulation of electrons. Dotted contours indicate a negative value, i.e. a dearth of electrons. The bunching of the particles yields a chain of ellipses centered on the phase velocity $\mathrm{v_p}$ and zeroes of the potential, which is shown in the rightmost panel. The panel marked δn displays both the resistive (thick line) and reactive (thin line) components of the density perturbation. It is clear that the linear perturbation is mostly resistive. In addition, from the maxima of δn being in phase with $\partial\phi/\partial x > 0$ we can conclude that the wave accelerates the electrons, whereby it is being damped. This is consistent with the power-law model, $F(v) \sim v^{-4}$, we have chosen for drawing the plot.

Note the slight tilt of the ellipses in Fig. 13.2. A consequence is that the result of a velocity-integration of the perturbed distribution critically depends on the integration window's width and centering. For computing δn shown

in the mid-panel we used a 7% width on either side of v_p. However, if the window is narrower and not centered on v_p, the integration will emphasize the reactive component. Furthermore, the sign of the latter depends upon whether the window happens to be centered a little above or below v_p.

In Fig. 13.2 the parameter μ is small, $\mu = 0.09$, hence the interaction is justifiably in the linear regime. However, when either the wave amplitude is larger or the packet is more extended, the linear solution to the Vlasov equation loses its validity and one must account for nonlinear corrections. These corrections to the orbits of resonant electrons δv and δx are difficult to compute analytically. Instead, we resort to particle-in-cell simulations, where consistent interactions between field and particles are automatically taken into account. The results of these simulations are shown in Fig. 13.3 which display the bunch-ellipses in a weakly nonlinear regime with $\mu = 1.2$. Solid contours and shaded areas indicate a positive value, or an accumulation of electrons. Dotted contours indicate a negative value, or a dearth of electrons. Two points must be noted. First, the wave is here driven by a bump on the tail of the distribution function. Accordingly, resonant electrons are decelerated

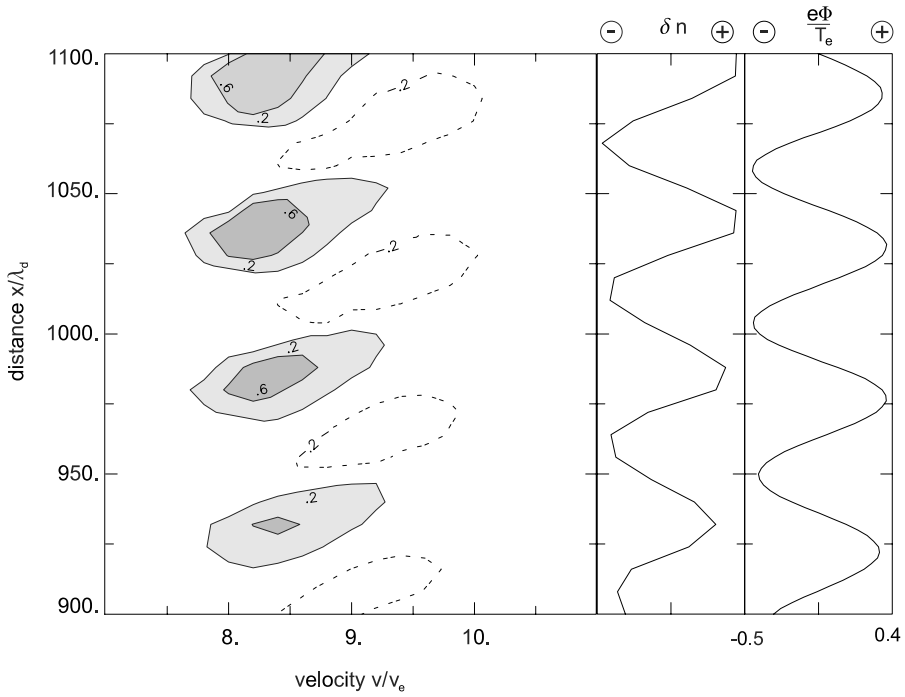

Fig. 13.3. Bunch-ellipses in a weakly nonlinear regime, from a particle-in-cell simulation where the Langmuir packet is amplified by a bump on tail located at $v = 10v_e$. Here $\mu = 1.2$ and $v_p = 8.7v_e$. Accumulation locales (*shaded in gray*) have decelerated while dearth locales (*dashed contours*) accelerated. More in the text

by the wave and maxima of δn are in phase with $\partial\phi/\partial x < 0$. Second, since bunches of accumulated electrons are decelerated, the nonlinear correction to their orbit has $\delta v < 0$ and $\delta x < 0$. In contrast, bunches associated with a dearth of electrons are accelerated and thus have $\delta v > 0$ and $\delta x > 0$. Hence, the two types of bunch-ellipses are no longer aligned at $v = \mathrm{v_p}$ as in Fig. 13.2. One can see in the plot that the solid contours have moved to the left while the dotted contours have moved to the right. In addition, their position in x drifts and slowly converges toward maxima of the potential, whereby their phase becomes more reactive.

13.3 Extended Wave Packet: A BGK Analysis

The only nonlinear term in the Vlasov-Poisson system of equations is the acceleration term on the right hand side of (13.2). In Sect. 13.2, we chose to linearize this term by splitting the distribution in a large, homogeneous part F and a small, inhomogeneous part f, and then neglecting $\partial f/\partial v$ versus $\partial F/\partial v$. We found that this was justified as long as $\mu \ll 1$. However, when the wave packet is so extended that a traversing electron can satisfy the resonance condition for a long time, this electron can be significantly accelerated by the electric field. Its orbit is then deeply altered. Therefore, the distribution function is strongly modified and the linearization procedure breaks down.

The BGK method offers another approach to solving the Vlasov-Poisson system of equations. Let us now imagine a very long wavepacket and examine the phase-space orbits of electrons in the so-called waveframe (frame moving with the wave phase velocity). These orbits are determined by the energy of the electrons

$$w = v^2/2 - \phi(x) \quad \text{where } E(x) = -\frac{\partial\phi}{\partial x} \ . \tag{13.14}$$

For this section, in order to simplify the notation, we introduce dimensionless units where length is normalized by λ_d, velocity is normalized by the electron thermal velocity $v_e = \sqrt{T_e/m}$, and the electrostatic potential is normalized by T_e/e. Electrons with $w < 0$ are trapped in local maxima of the wave potential. Electrons with $w > 0$ are untrapped and alternately accelerate and decelerate while passing over hill and dale of the potential. Now, any function of w where $\phi(x)$ is time-independent automatically satisfies Vlasov equation. The BGK approach exploits that property and assumes that the distributions are function of w only and that they are in a self-consistent steady state with the potential. This enables one to concentrate on solving the Poisson equation for a given model of wave field, e.g. here a sinusoidal wave

$$\phi(x) = \Psi \sin kx \, . \tag{13.15}$$

Let $F_e(w)$ and $F_t(w)$ be the distribution functions of, respectively, the passing and the trapped electrons. Poisson equation reads

$$\frac{d^2\phi}{dx^2} = -n_i + \int_{\Psi}^{\infty} \frac{F_e^+(w) + F_e^-(w)}{\sqrt{2}(w+\phi)^{1/2}} dw + \int_{-\phi}^{\Psi} \frac{\sqrt{2}F_t(w)}{(w+\phi)^{1/2}} dw \,. \tag{13.16}$$

Terms on the right hand side represent, in order, the density of the ions, which are supposed to form a constant background, the density contribution from the passing electrons, and that from the trapped electrons. The passing electrons have been split into those moving to the right, $F_e^+(w)$, and those moving to the left, $F_e^-(w)$. The trapped electrons, by contrast, must be symmetric with the same flux of right and left moving particles, $F_t^+(w) = F_t^-(w) = F_t(w)$, in a stationary situation.

13.3.1 Passing Electrons

A model of distribution for the ambient electrons that is practical for computational purposes and representative of the observed distributions is given by

$$F_e^{\pm}(v) = \frac{2}{\pi} \frac{1}{[1 + (v \pm v_p)^2]^2} \,, \tag{13.17}$$

where v is an absolute number measuring the velocity from the wave frame, and the direction is selected by the $\pm$ sign. Note that this distribution is normalized to unity and becomes a power-law in v^{-4} at large velocities. In the presence of the wave it translates into

$$F_e^{\pm}(w) = \frac{2}{\pi \left[1 + \left(\sqrt{2}(w-\psi)^{1/2} \pm v_p\right)^2\right]^2} \quad \text{with } w > \Psi \,. \tag{13.18}$$

After integrating this expression for the densities of right and left moving particles, one obtains the total density of passing electrons as

$$n_p = 1 - \frac{2}{\pi} \frac{\sqrt{\varphi}\,(1 + \varphi - v_p^2)}{v_p^4 + 2v_p^2(1-\varphi) + (1+\varphi)^2} - \frac{1}{\pi} \arctan\left(\frac{2\sqrt{\varphi}}{v_p^2 + 1 - \varphi}\right) \tag{13.19}$$

where the notation $\varphi \equiv 2(\Psi + \phi)$ is introduced. The density is maximum where the potential is minimum, at $\varphi = 0$, and monotonically decreases toward a minimum where the potential is maximum, at $\varphi = 4\Psi$. We will assume that $4\Psi \ll 1$, which enables us to expand the complicated expression above into the simpler

$$n_p(\phi) = 1 - \frac{4\sqrt{2}}{\pi(v_p^2+1)^2}(\Psi + \phi)^{1/2} - \frac{16\sqrt{2}(5v_p^2 - 1)}{3\pi(v_p^2+1)^4}(\Psi + \phi)^{3/2} \tag{13.20}$$

The most important term, in $\varphi^{1/2}$, has a coefficient that is related to the value of the ambient distribution at the wave phase velocity ((13.17) with $v = 0$). This is in agreement with the intuitive idea that electrons which move slowly along the separatrix (located at $v = \sqrt{2\Psi(1 + \sin kx)}$) are strongly affected by the potential and thus contribute the most to the density variations. By contrast, fast-moving electrons far from the separatrix hardly "notice" the potential and pass by quasi undisturbed.

13.3.2 Trapped Electrons

We formally define the density of trapped electrons n_t as an unknown function of ϕ through the expression

$$n_t(\phi) \equiv \int_{-\phi}^{\Psi} \frac{\sqrt{2}F_t(w)}{(w+\phi)^{1/2}} dw \; . \tag{13.21}$$

This integral equation can be inverted for $F_t(w)$, which yields

$$F_t(w) = \frac{1}{\sqrt{2}\pi} \int_{-\Psi}^{-w} \frac{1}{(-w-\phi)^{1/2}} \; \frac{d}{d\phi} n_t(\phi) \; d\phi \; . \tag{13.22}$$

The potential $\phi(x)$ is given by (13.15) and requires a net density perturbation

$$n_s(\phi) = -k^2\phi \quad \text{with} \quad n_s = n_p + n_t \; . \tag{13.23}$$

Substituting n_s and n_p for n_t in (13.22), one obtains after integration

$$F_t(w) = \frac{2}{\pi(v_p^2+1)^2} - \frac{\sqrt{2}}{\pi v_p^2}(\Psi - w)^{1/2} + \frac{4(5v_p^2-1)}{\pi(v_p^2+1)^4}(\Psi - w) \tag{13.24}$$
$$\text{with} \qquad -\Psi \leq w < \Psi \; .$$

This is an explicit expression for the distribution of trapped electrons that is consistent with a sinusoidal wave. Due to the v_p^8 dependence in the coefficient's denominator, the third term is considerably smaller than the second. Thus, the sign of the second term indicates that the distribution is punctuated with periodic holes located where $(\Psi - w)$ maximizes, namely at maxima of the potential ϕ.

An illustration of the perturbed distribution is provided in Fig. 13.4. It has been recast in terms of x and v in the plasma frame and normalized to $f_e(v_p)$. The display is similar to Figs. 13.2 and 13.3, including the potential in the right panel. Gray shadings indicate the phase space density with light grays denoting depletion. Clearly, a velocity integration by means of a window centered on v_p will provide a density perturbation δn which is (1) reactive and (2) characterized by $\delta n < 0$ where ϕ is maximum.

13.4 Electron Phase Sorting Measurements

The predictions of the theory of Langmuir wave interaction with electrons raise the question of experimental tests of the theory. In particular, measurements of the portion of the electron distribution which is resonant with the waves along with measurements of the waves themselves permits detailed comparison of theory and data which probes the success of these models..

The past 15–20 years have seen the development of wave-particle correlators which sort individual electron counts into bins corresponding to the phase

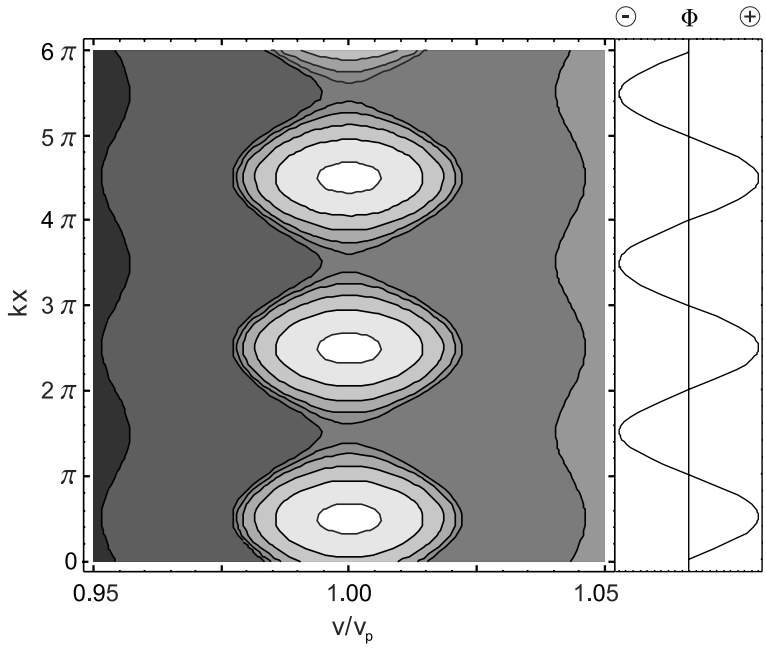

Fig. 13.4. BGK solution showing the perturbed distribution in a self-consistent state with an infinite wave train $\phi(x) = \Psi \sin kx$. Phase space density is indicated by gray shadings where darker gray means more particles. Clearly, integrating over a velocity window around v_p produces a reactive signal with density minima in phase with maxima of the potential and vice versa

of the observed wave as each electron arrives at the payload. The advantage of instrumentation of this type is that by accumulating the sorted electron counts over many wave periods, the average phase relation of the electrons relative to the wave can be determined for a relatively modest usage of spacecraft telemetry bandwidth. In this way, key aspects of the detailed physical interaction of Langmuir waves and electrons can be studied as never before.

13.4.1 Measurements of the Resistive Component

The first electron phase sorting correlator which measured the electron to Langmuir wave phase relation was developed at UC Berkeley in the late 1980's for use on auroral sounding rockets. The principle of operation is illustrated in the schematic shown in Fig. 13.5.

The incoming waveform from the parallel electric field antenna is first passed through a bandpass filter to remove signals outside the frequency range expected for Langmuir waves. At rocket altitudes in the auroral zone, this corresponds to a 200 kHz-5 MHz band. By removing frequencies outside this range, any significant signal remaining has high likelihood of being that from

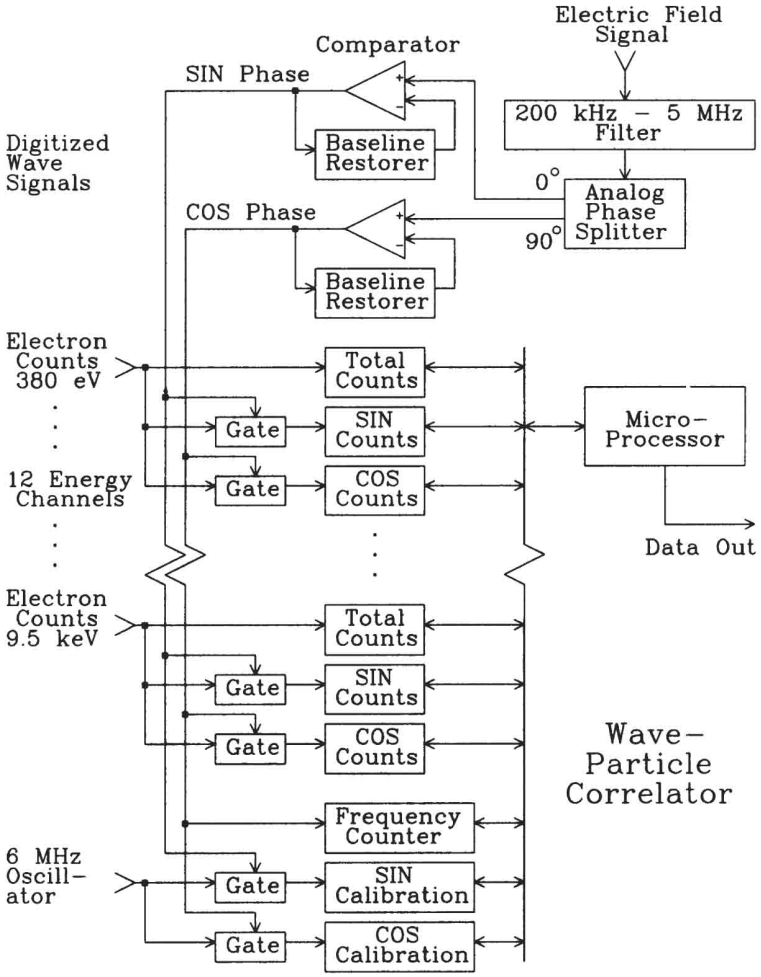

Fig. 13.5. Schematic diagram of the UC Berkeley electron phase sorting correlator from the work of Ergun et al. [9]. The instrumentation sorted electron into two phase bins of 180° width, one centered on 0° phase and one centered on 90° phase. By combining these bins with total counts over the entire interval, the phase of electrons could be determined within four 90° intervals (Reprinted with permission from American Geophysical Union)

Langmuir waves. After this filter, the signal was then passed through an analog phase splitter to produce one signal with no phase shift and an identical signal shifted by 90° in phase. Each of these two signals was then passed through a comparator to produce a one-bit digitization of the signal. Because the count rate of phase-bunched electrons is typically a small fraction of the total electron count rate (of the order of 1%), it is essential that this digitized signal

have a precise 50% duty cycle so as not to bias the results. This was ensured through the use of a baseline restoring circuit which monitored the integrated digitized signal as a function of time and adjusted the baseline of the incoming analog signal to yield an accurate 50% duty cycle.

The two digitized signals, dubbed SIN for the 0° phase signal and COS for the 90° signal, were used to sort electrons at several fixed energies as they arrived at the rocket payload. When a given signal was high, the counter was gated open and allowed to accept incoming electron counts. When the signal was low, the counter was gated closed and would not accept electron counts. In this way, counts were accumulated over the 180° phase interval centered on 0° phase (the COS counter) and over the 180° phase interval centered on 90° phase (the SIN counter). In addition to these two counters, a third counter accumulated counts over the entire wave period. The set of three counters was duplicated 12 times to analyze electron counts from 12 fixed energy channels of a fast electron spectrometer that was oriented to detect electron precipitation parallel to the magnetic field.

Under the assumption that the phase correlation of the electrons is sinusoidal, the square root of the sum of the squares of the SIN and COS channels yields the amplitude of the correlation. The phase of the correlation is then the opposite of the inverse tangent of the ratio of the SIN and COS counters.

In analyzing correlator results, it is important to consider how random fluctuations in counting rate can influence the results. Poisson statistics can give significant variations away from the average count particularly for small numbers of counts. Thus it is essential to analyze correlation data in terms of standard deviations σ away from the expected background. In terms of standard deviations, the probability of 2σ variation is once in 22 samples and is generally not considered significant. A 3σ variation is expected to occur once in every 370 measurements. However, a 3.5σ variation should occur only once every 2149 samples and 4σ events occur only once every 15783 samples. Thus to be considered truly significant, events with $\sigma > 3.5$ are preferred.

The correlator was flown on a rocket launched from Poker Flat, Alaska on March 4, 1988 which crossed several auroral arcs during the expansion phase of substorm. During the flight, the parallel component of the electric field reached amplitudes of 100 mV/m in the frequency band from 200 kHz to 5 MHz with a dominant frequency of 1.4 MHz indicating the presence of strong Langmuir oscillations. The output of the correlator showed several events with significant correlation with electrons from the eight lowest energy channels which covered a range of energies from 380 eV to 3.2 keV. The correlations appeared first in the higher energy channels and then moved to lower energy.

Analysis of the data from this rocket flight yielded five events with fluctuations greater than 4σ. These five events, plotted as function of wave electric potential, are shown in Fig. 13.6 taken from Ergun et al. [9].

Each event is plotted with the associated error bar as determined from experimental uncertainties as well as the 1σ statistical error of the counts. All five events are located near 90° or 270° with respect to the wave electric

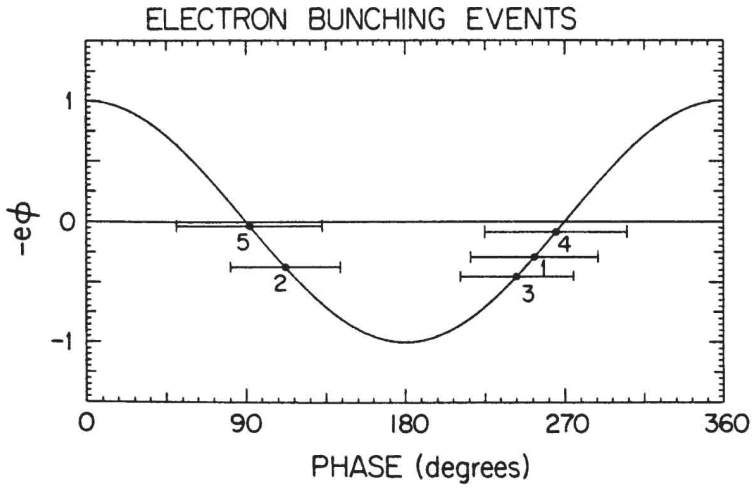

Fig. 13.6. Phase of bunched electrons for five events of correlations at levels greater than 4σ from Ergun et al. [9]. The phase of each event is plotted along with error bars derived from experimental uncertainties (Reprinted with permission from American Geophysical Union)

potential. This corresponds to 0° or 180° with respect to the wave electric field. The frequency of all 5 events was 1.4 MHz which, when combined with the electron energies of 380 eV to 3.2 keV, yields wavelengths of 8 m to 20 m. Events 2 and 5 were such that more electrons were being accelerated by the wave than were being decelerated and thus corresponds to wave damping. They occurred during periods of weaker amplitudes of 10–20 mV/m. Events 1, 3, and 4 had more electrons decelerating than accelerating corresponding to wave growth. At these times the wave amplitudes were near 100 mV/m or greater.

Following the analysis of Sect. 13.2, the value of μ can be calculated using the observed electric field amplitude of 80 mV/m, the inferred wavelength $\lambda = 12.8$ m, and observed the plasma frequency of 1.4 MHz along with a value for kL. For these events, kL was estimated to be of the order of $kL = 30$ which yields a value of $\mu = 0.09$. This is consistent with the linear analysis for a short wave packet which predicts the observation of the resistive component of the electron perturbation because in this regime, the resistive perturbation is generally larger than the reactive perturbation as illustrated in Fig. 13.2.

13.4.2 Measurements of the Reactive Component

Further improvement in the measurement of the phase of electron bunching in Langmuir waves in the auroral zone was achieved using a new phase correlator developed at the University of Iowa (UI) in the late 1990's. Figure 13.7 shows

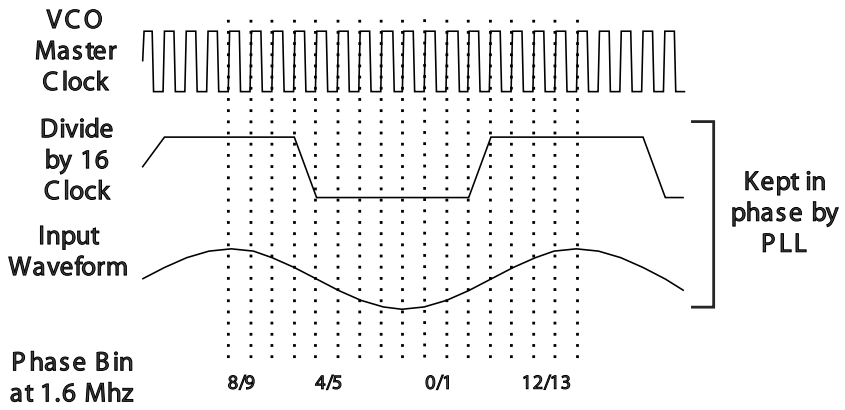

Fig. 13.7. The UI wave-particle correlator uses a phase-locked loop (PLL) locked to the measured waveform with a clock derived from master voltage-controlled oscillator (VCO) running at 16 times the frequency. This master clock subdivides the wave in 16 phase bins. Electron counts are sorted into the bins as they arrive to produce a map of phase bunching (Reprinted with permission from American Geophysical Union)

the principle of operation. The correlator used a voltage-controlled oscillator (VCO) running at 16 times the expected frequencies for Langmuir waves.

The VCO clock signal was divided by 16 to provide a signal which was then aligned to the measured AC parallel electric field through the use of a phase-locked loop (PLL). The PLL output a signal which indicated when the loop was properly locked and also the frequency of the locked signal which is then compared with the analog waveform data to ensure that the PLL was locked to signals of interest. Because the VCO master clock runs at 16 times the frequency of the wave to which the PLL is locked, it provides a highly accurate means of sub-dividing the measured wave into 16 phase bins. As electrons are counted by the detectors, they are sorted into the appropriate phase bin associated with their arrival time. Calibration of the detector, wave, and correlator electronics verified the accuracy of the phase bins and determined the timing delays through the system. The timing delays cause the absolute bin number which corresponds to 0° phase shift (as well as other phase angles) to shift as a function of input wave frequency. For example, at 1.6 MHz, 0° phase shift between the wave and the electrons occurs between correlator bins 8 and 9. The bottom of Fig. 13.7 shows the calibrated phase angles of the bins at a frequency of 1.6 MHz.

The UI correlator was flown on a rocket flight which was launched from Poker Flat, Alaska in February 6, 2002. Strong Langmuir waves were observed as the rocket traversed an auroral form near the poleward boundary of the auroral precipitation. The Langmuir waves were associated with a burst of field-aligned electrons at energies below 1 keV and well below the inverted-V

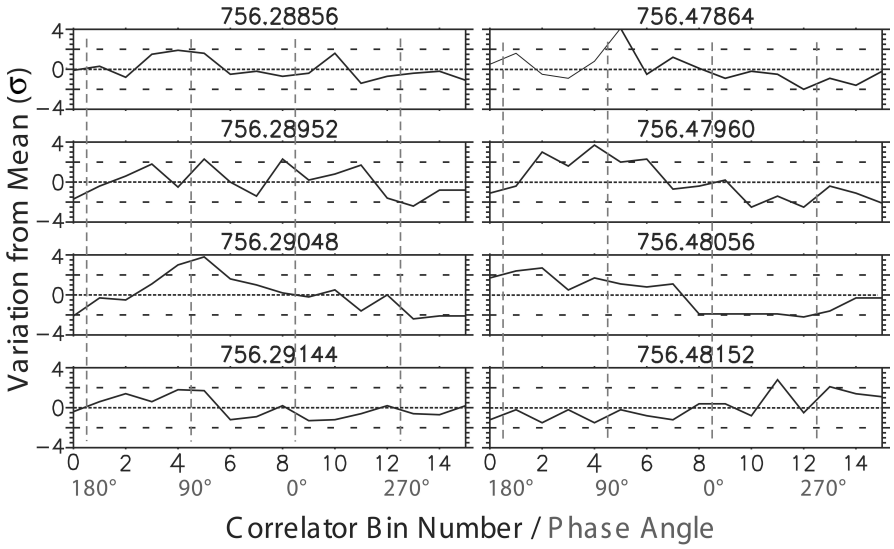

Fig. 13.8. Two examples of significant correlation of Langmuir waves with electrons at 468 eV. For each of the 16 phase bins, the count level is shown in terms of standard deviations away from the average number of counts that would be expected for a bin for the total number of counts received (Reprinted with permission from American Geophysical Union)

peak energy of 5 keV. During this period of Langmuir emission, two intervals of stronger emission with amplitudes of 60–200 mV/m were observed. Each of these intervals were of the order of 50 ms in duration. During both intervals, the field-aligned wave power was 8.5–11 times that of the perpendicular power indicating field-aligned waves. Because the payload telemetered continuous waveform data, it was possible to determine that the Langmuir waves were remarkably monochromatic with little or no variation in frequency. During each of the two larger amplitude bursts, the amplitudes varied slowly over hundreds of wave periods.

During each of the two bursts of strong Langmuir waves, significant wave-particle correlation was found as shown in Fig. 13.8.

Each set of panels shows four consecutive sets of correlator measurements of electrons with energy of 468 eV and which were sampled every millisecond. Data are plotted as standard deviations away from the expected average count rate in each phase bin. To be regarded as significant, we require a correlation level of at least 3.5σ. Although there is frequent variation of the order of 2σ shown in Fig. 13.8, these are not considered significant because the probability of 2σ variation is once in 22 samples as discussed above. With this in mind, in the left set of panels, the first and third panels show notable correlation. The first panel shows a weakly significant correlation with three adjacent phase bins with $\sim 2\sigma$ levels of correlation corresponding to a 3.3σ variation.

However, the third panel from the top has two consecutive phase bins with phase bunching above 3σ. The combined probability of two such bins occurring together exceeds that of a single 4σ event. The bins in which the phase bunching occurs are those at 90° with respect to the wave electric field (positive away from the ionosphere) for the wave frequency of 1.6 MHz.

The second example shown in the right set of panels in Fig. 13.8 shows a second event with similar high levels of significance in the top three panels. Initially, a single channel with more than 4σ significance occurs at 90°. In the second panel, this feature broadens and shifts to somewhat larger phase shift with four phase bins above 2σ representing a combined significance of more than 4σ. The calculated probability of random occurrence of the counts represented by the four phase bins centered around 90° is one in 932,068 suggesting that this is a highly significant correlation. The third panel shows further advance to larger phase angles, with most significant set of signals now showing more than -4σ (5 channels at -2σ each) between 270° and 0°.

Figure 13.9 shows three sequential distribution function plots from immediately before, during and immediately after the first correlation event. The times given above each plot correspond to the center time of each 40 ms energy sweep. As can be seen, at the time of the correlation, a small, downward electron beam parallel to the magnetic field is measured at the same energy as the correlated electrons. This is indicated by a small arrow at the velocity corresponding to 468 eV. The isolated beam is not present in the distribution function measured before the correlation or in the distribution measured after the correlation. Although the time resolution of these measurements is much lower than for the correlator, this suggests that the correlation arises from this beam.

The brief increase in electron phase space density at the energy of correlated electrons illustrated in Fig. 13.9 was also seen for the second correlation event. In both cases the preceding and following energy sweeps did not show this feature, suggesting that the resonant electrons were only briefly in the detectable energy range. From the energy of the correlated electrons (468 eV) and the frequency of the waves (1.6 MHz), we can derive the wavelength of the Langmuir waves as 8.2 m, similar to the results of the UC Berkeley measurements.

The waveform data makes it possible to estimate the packet parameters to aid in the interpretation of correlation events. Figure 13.10 shows 15 ms of data which includes the interval of the second set of correlations.

The interval during which the correlations were observed is indicated by a heavy line above the waveform data. As can be seen, the correlations occurred during the largest wave amplitudes. If we assume a background thermal energy of 0.2 eV and use the inferred wavelength of 8.2 m along with the observed Langmuir frequency of 1.6 MHz, then the group velocity for Langmuir waves,

$$v_g = \frac{\partial \omega}{\partial k} \simeq \frac{3v_{th}^2 k}{\omega_{pe}} = \frac{3v_{th}^2}{\lambda f_{pe}} \,, \tag{13.25}$$

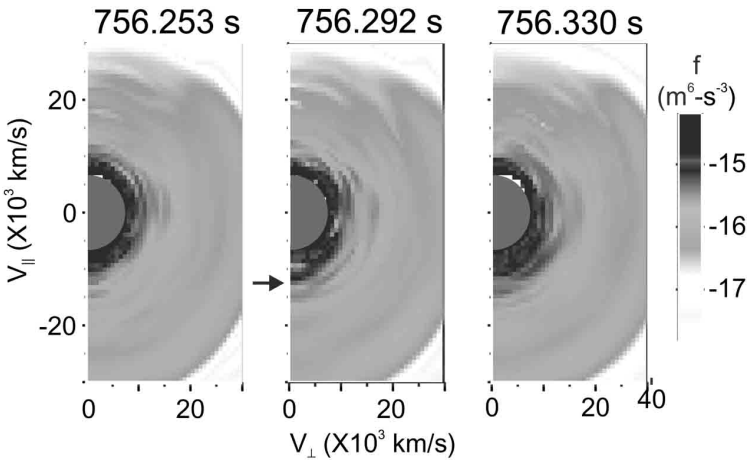

Fig. 13.9. Sequential distribution functions from before, during, and after the correlation event shown in the left panel of Fig. 13.8. The velocity corresponding to the correlated electrons is indicated with an arrow in the middle panel and shows that a field-aligned beam is present at this time (Reprinted with permission from American Geophysical Union)

gives the value of $v_g = 8.02$ km/s = 8 m/ms. If the wave is traveling down the field line, then the amount of the wave packet above the correlation observations extends from the time of the correlations in Fig. 13.10 to the end of the packet some 3 ms later. This yields a length of the wavepacket above rocket payload of 24.1 m at the time of the correlations and corresponds to a value of $kL = 18.5$. A rough average for the amplitude of the electric field during this interval is 130 mV/m. Combining this with the estimate of kL gives a value of $\mu = 0.12$, consistent with the linear theory and similar to the value used in Fig. 13.2.

It should be pointed out, however, that the usual limitations of single point spacecraft measurements apply to this interpretation. With the data at hand, we cannot rule out a scenario in which the electron beam has suddenly appeared and the wave packet has grown over time at the spacecraft location. Indeed, such a scenario would be consistent with the quasi-exponential increase in amplitude of the packet in the 10 ms preceding the correlation observations. In this case, there is no way to ascertain the amount of wave packet above the payload, but the shape of the packet suggests that the correlations were observed shortly after the linear growth phase ended and some type of non-linear saturation began to operate. The group velocity calculation still applies, but now becomes a lower bound on the length of the packet. By observing the packet for 3 ms we know that it extended at least 24 m above the rocket, but it may have extended much further, and then disappeared due to temporal effects in the driving electron distribution. A third alternative is that the payload may have moved into and then out of a pre-existing region

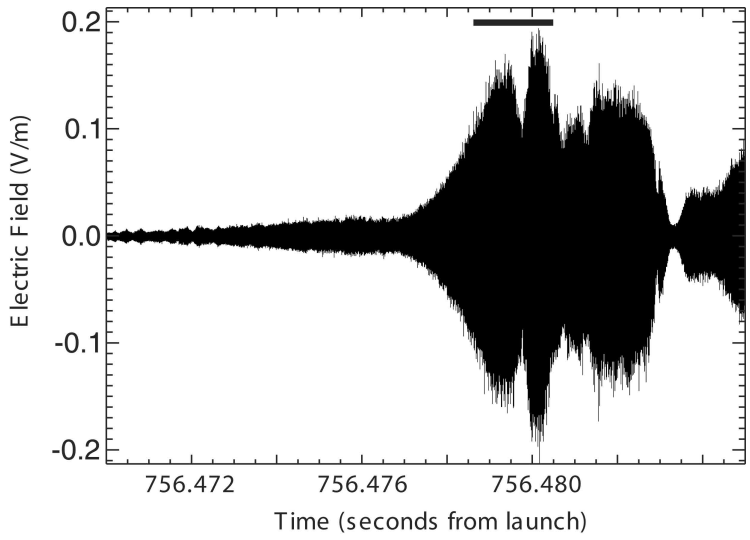

Fig. 13.10. Langmuir waveform data which includes the interval of the second set of correlation events. The correlation interval is indicated by the solid bar above the waveform

of Langmuir waves such that the observed wave envelope is determined by the spatial structure of the Langmuir waves along the rocket track. However, given the rocket velocity of roughly 1 km/s, this latter scenario would require a rather small wave packet and does not seem likely.

13.5 Discussion

The electron correlator observations reported by the UC Berkeley were predominantly resistive, that is, in-phase or 180° out-of-phase with the wave electric field. Although they had expected to see the reactive component, the observations of the resistive component prompted the analysis developed in Sect. 13.2 and led to the conclusion that they had observed electrons which were bunched by relatively short wave packets with kL of the order of 50–100. This result was also consistent with the value for μ that was determined which suggested that thee observed waves were in the linear regime.

As shown in the middle panel of Fig. 13.2, for $\mu = 0.09$, the perturbation to the density and hence, to the electron distribution, is dominated by the resistive component for small values of μ. Although the reactive component is present, as shown in Fig. 13.1, its bipolar character requires relatively narrow response electron detectors so as not to average the positive and negative perturbation together, yielding no perturbation. The detectors which made these resistive correlator measurements had $\Delta v/v \simeq 16\%$ and as shown in

Fig. 13.1, this is broader than the expected perturbation relative to the phase velocity.

The electron phase bunching observed by the UI group was predominantly 90° out-of-phase with the electric field, suggesting a trapped population of electrons. The wave field in which the phase-bunched electrons were observed was long-lived in terms of wave periods, monochromatic, and showed slow modulation of the wave envelope. As discussed above, using the assumption that the wave packet moved past the payload due the group velocity of the waves yields a low value of μ which would suggest that the linear analysis also applies to this case. In examining Fig. 13.2, it is seen that although the overall perturbation to the density has a greater resistive component than reactive component, the reactive component does exist. On closer examination of Fig. 13.2, however, it can be seen that for a narrow range of velocities of the order of $\Delta v/v = 5\%$, on either side of the phase velocity, the reactive component is more dominant. This is seen in the shifting of the perturbed distribution toward being in phase with the potential for velocities above the phase velocity and a shift toward 180° out-of-phase for velocities below the phase velocity. Because the UI electron detectors had a comparably narrow velocity response $\Delta v/v \simeq 5\%$, they are capable of capturing one or the other side of the perturbation and could measure a reactive perturbation even for a short wave packet.

In the case that the envelope of the observed waves is predominantly due to temporal evolution, then it is likely that the wave packet extends a significant distance above the rocket payload. This is suggested by the fact that the electron distribution will be unstable over a wide range of altitudes and would be expected to grow waves over a region of many wavelengths in extent. The character of the wave envelope also suggests a transition away from the linear stage of growth. Taken together, these two arguments suggest that an alternative explanation is that the correlations indicate trapping and thus the BGK analysis is appropriate. As shown in the right hand panel of Fig. 13.3, when the electron-Langmuir wave interaction becomes nonlinear, the density perturbation shifts toward a purely reactive phase as the electrons become trapped. Indeed the bunching of the electrons observed by the UI group is such that the positive perturbation was that of trapped electrons.

To resolve this ambiguity will require future experiments which provide adjacent energy channels with narrow response so that the full character of the perturbed distribution function can be revealed. This would allow one to see if both reactive pieces, that is the positive perturbation below the phase velocity and the negative perturbation above the phase velocity shown in Fig. 13.1, are observed side-by-side as the linear model would suggest or if only a single reactive perturbation is observed, consistent with the BGK analysis.

13.6 Conclusions

Multiple spacecraft observations have confirmed the ubiquitous nature of Langmuir waves in the presence of auroral electrons. Early observations have shown clear evidence that the electrons show variations consistent with bunching at or near the Langmuir frequency. Linear analysis of the interaction of a finite Gaussian packet of Langmuir waves shows that there are two components to the perturbation to the electron distribution function, one in-phase (or 180° out-of-phase) with respect to the electric field called the resistive component and one which is 90° (or 270°) out-of-phase with respect to the electric field. For small wave packets, the resistive perturbation dominates. For longer wave packets, a non-linear analysis is appropriate which suggests that the electrons have interacted long enough to become trapped and the reactive phase becomes dominant.

Rocket observations of the phase bunching of the electrons using wave-particle correlators have measured both components. The UI observations [Kletzing et al., 16] differ from those of the UC Berkeley observations [Ergun et al., 7, 9] in that a purely reactive phase bunching was observed as compared to a predominantly resistive perturbation. The resistive phase results of the UC Berkeley group were interpreted as arising from a short wave packet. The UI observations of the reactive phase can be explained by either a long, coherent train of Langmuir waves or that the narrower velocity response of the UI detectors made it possible to capture only one side of the reactive component of the perturbed distribution function for a short wave packet in the linear regime. Future wave-particle correlator experiments should be able to resolve these questions by providing more examples with better velocity space coverage.

References

[1] Bale, S.D.: Observation of the topside ionospheric mf/hf radio emission from space, Geophys. Res. Lett. 26, 667, 1999.
[2] Bauer, S.J. and R.G. Stone: Satellite observations of radio noise in the magnetosphere, Nature 218, 1145, 1968.
[3] Beghin, C., J.L. Rauch, and J.M. Bosqued: Electrostatic plasma waves and hf auroral hiss generated at low altitude, J. Geophys. Res. 94, 1359, 1989.
[4] Boehm, M.H.: *Waves and static electric fields in the auroral acceleration region*, PhD thesis, University of California, Berkeley, 1987.
[5] Boehm, M.H., G. Paschmann, J. Clemmons, H. Höfner, R. Frenzel, M. Ertl, G. Haerendel, P. Hill, H. Lauche, L. Eliasson, and R. Lundin: The tesp electron spectrometer and correlator (F7) on Freja, Space Sci. Rev. 70, 509, 1995.
[6] Bonnell, J.W., P.M. Kintner, J.E. Wahlund, and J.A. Holtet: Modulated langmuir waves: observations from freja and scifer, J. Geophys. Res. 102, 17233, 1997.

[7] Ergun, R.E., C.W. Carlson, and J.P. McFadden: Wave-particle correlator instrument design, In: R.F. Pfaff, J.E. Borovsky, and D.T. Young (Eds.), *Measurement Techniques in Space Plasmas: Particles*, volume 102 of AGU Geophys. Monogr. Ser., p. 4325, AGU, Washington, D.C., 1998.
[8] Ergun, R.E., C.W. Carlson, J.P. McFadden, J.H. Clemmons, and M.H. Boehm: Evidence of a transverse modulational instability in a space plasma, Geophys. Res. Lett. 18, 1177, 1991.
[9] Ergun, R.E., C.W. Carlson, J.P. McFadden, D.M. TonThat, J.H. Clemmons, and M.H. Boehm: Observation of electron bunching during Landau growth and damping, J. Geophys. Res. 96, 11371, 1991.
[10] Gough, M.P., P.J. Christiansen, and K. Wilhelm: Auroral beam-plasma interactions: particle correlator investigations, J. Geophys. Res. 90, 12287, 1990.
[11] Gough, M.P. and A. Urban: Auroral beam/plasma interaction observed directly, Plan. Space Sci. 31, 875, 1983.
[12] James, H.G., E.L. Hagg, and L.P. Strange: Narrowband radio noise in the topside ionosphere, *AGARD Conf. Proc.*, AGARD-CP-138, 24–1–24–7, 1974.
[13] Kelley, M.C. and G.D. Earle: Upper hybrid and Langmuir turbulence in the auroral *e*-region, J. Geophys. Res. 93, 1993, 1988.
[14] Kellogg, P.J. and S.J. Monson: Radio emissions from the aurora, Geophys. Res. Lett. 6, 297, 1979.
[15] Kintner, P.M., J. Bonnell, S. Powell, and J.E. Wahlund: First results from the freja hf snapshot receiver, Geophys. Res. Lett. 22, 287, 1995.
[16] Kletzing, C.A., S.R. Bounds, J. LaBelle, and M. Samara: Observation of the reactive component of langmuir wave phase-bunched electrons, Geophys. Res. Lett., 32, L05106, doi:10.1029/2004GL021175, 2005.
[17] McAdams, K.L. and J. LaBelle: Narrowband structure in hf waves above the electron plasma frequency in the auroral ionosphere, Geophys. Res. Lett. 26, 1825, 1999.
[18] McAdams, K.L., J. LaBelle, M.L. Trimpi, P.M. Kintner, and R.A. Arnoldy: Rocket observations of banded stucture in waves near the langmuir frequency in the auroral ionosphere, J. Geophys. Res. 104, 28109, 1999.
[19] McFadden, J.P., C.W. Carlson, and M.H. Boehm: High-frequency waves generated by auroral electrons, J. Geophys. Res. 91, 12079, 1986.
[20] Muschietti, L., I. Roth, and R. Ergun: Interaction of Langmuir wave packets with streaming electrons: phase-correlation aspects, Phys. Plasmas 1, 1008, 1994.
[21] Newman, D.L., M.V. Goldman, and R.E. Ergun: Langmuir turbulence in the auroral zone 2. nonlinear theory and simulations: J. Geophys. Res. 99, 6377, 1994.
[22] Nicholson, D.R.: *Introduction to Plasma Theory*, Wiley, New York, 1983.
[23] Reiner, M.J. and M.L. Kaiser: Complex type iii-like radio emissions observed from 1 to 14 mhz, Geophys. Res. Lett. 26, 397, 1999.
[24] Reiner, M.J., M. Karlicky, K. Jiricka, H. Aurass, G. Mann, and M.L. Kaiser: On the solar origin of complex type iii-like radio bursts observed at and below 1 mhz, Astrophys. J. 530, 1049, 2000.
[25] Samara, M., J. LaBelle, C. A. Kletzing, and S.R. Bounds: Rocket observations of structured upper hybrid waves at $f_{uh} = 2f_{ce}$, Geophys. Res. Lett., submitted, 2004.

[26] Sanbonmatsu, K.Y., I. Doxas, M.V. Goldman, and D.L. Newman: Non-Markovian electron diffusion in the auroral ionosphere at high Langmuir-wave intensities, Geophys. Res. Lett. 24, 807, 1997.
[27] Spiger, R.J., J.S. Murphree, H.R. Anderson, and R.F. Loewenstein: Modulation of auroral electron fluxes in the frequency range 50 kHz to 10 MHz, J. Geophys. Res. 81, 1269, 1976.
[28] Stasiewicz, K., B. Holback, V. Krasnoselskikh, M. Boehm, R. Boström, and P.M. Kintner: Parametric instabilities of langmuir waves observed by freja, J. Geophys. Res. 101, 21515, 1996.
[29] Walsh, D., F.T. Haddock, and H.F. Schulte: Cosmic radio intensities at 1.225 and 2.0 mc measured up to and altitude of 1700 km, Space Res. 4, 935, 1964.
[30] Weatherwax, A.T., J. LaBelle, M.L. Trimpi, and R. Brittain: Ground-based observations of radio emissions near $2f_{ce}$ and $3f_{ce}$ in the auroral zone, Geophys. Res. Lett. 20, 1447, 1993.